1 **Optimization of electrocatalytic H₂O₂ production at pilot plant scale**

2 **for solar-assisted water treatment**

3 Irene Salmerón [a,b], Konstantinos V. Plakas [c], Ignasi Sirés [d], Isabel Oller [a,b,*],

4 Manuel I. Maldonado [a,b], Anastasios J. Karabelas [c], Sixto Malato [a,b]

5 [a] *Plataforma Solar de Almería-CIEMAT, Ctra Senés km 4, 04200 Tabernas (Almería), Spain*

6 [b] *CIESOL, Joint Centre of the University of Almería-CIEMAT, 04120 Almería, Spain*

7 [c] *Chemical Process and Energy Resources Institute, Centre for Research and Technology – Hellas*

8 *(CERTH), 6th Km Charilaou-Thermi Road, Thermi, Thessaloniki GR 57001, Greece*

9 [d] *Laboratori d'Electroquímica dels Materials i del Medi Ambient, Departament de Química Física,*

10 *Facultat de Química, Universitat de Barcelona, Martí i Franquès 1-11, 08028 Barcelona, Spain*

11

13 *Corresponding author: E-mail address*: isabel.oller@psa.es (Isabel Oller)

Código de campo cambiado

14

Abstract

This manuscript summarizes the successful start-up and operation of a hybrid eco-engineered water treatment system, at pilot scale. The pilot unit, with 100-L capacity, has been devised for the efficient electrocatalytic production of H_2O_2 at an air-diffusion cathode, triggering the formation of $^{\bullet}OH$ from Fenton's reaction with added Fe^{2+} catalyst. These radicals, in combination with those formed at a powerful boron-doped diamond (BDD) anode in an undivided cell, are used to degrade a mixture of model pesticides. The capability of the plant to produce H_2O_2 on site was initially optimized using an experimental design based on central composite design (CCD) coupled with response surface methodology (RSM). This aimed to evaluate the effect of key process parameters like current density (j) and solution pH. The influence of electrolyte concentration as well as liquid and air flow rates on H_2O_2 electrogeneration and current efficiency at optimized j and pH was also assessed. The best operation conditions resulted in H_2O_2 mass production rate of 64.9 mg min^{-1}, 89.3% of current efficiency and 0.4 kWh m^{-3} of energy consumption at short electrolysis time. Performance tests at optimum conditions were carried out with 75 L of a mixture of pesticides (pyrimethanil and methomyl) as a first step towards the elimination of organic contaminants by solar photoelectro-Fenton (SPEF) process. The combined action of homogeneous ($^{\bullet}OH$) and heterogeneous (BDD($^{\bullet}OH$)) catalysis along with photocatalysis (UV photons collected at a solar CPC photoreactor) allowed the removal of more than 50% of both pesticides in 5 min, confirming the fast regeneration of Fe^{2+} catalyst through cathodic reduction and photo-Fenton reaction.

Keywords: Boron-doped diamond; Gas-diffusion electrode; Hydrogen peroxide electrogeneration; Solar photoelectro-Fenton; Wastewater treatment

1. Introduction

The extraordinary development of chemicals manufacturing and their widespread use in all human activities is intimately associated with contamination of aquatic environment. Water quality monitoring programs underline the seriousness of the problem worldwide and highlight the potential hazards posed by mixtures of synthetic organic contaminants (SOCs) and their metabolites in surface water and groundwater [1-4]. Typically, SOCs include solvents, preservatives, pharmaceuticals and personal care products, lubricants, dyes or active substances for plant protection [5]. Among the latter, methomyl (MET) and pyrimethanil (PYR) are ubiquitous in intensive agriculture, which is worrisome since they are classified as persistent organic pollutants (POPs) [6] and are considered extremely toxic [7,8]. This issue has prompted the application of advanced oxidation processes (AOPs) for the fast and complete removal of SOCs from polluted water streams [9], based on the in situ production of hydroxyl radical ($^{\bullet}OH$) as main reactive oxygen species (ROS).

Fenton's reaction between ferrous ions (Fe^{2+}) and hydrogen peroxide (H_2O_2), so-called Fenton's reagent, is the most popular source of $^{\bullet}OH$ for practical applications [10]. As an upgraded approach, the electro-Fenton (EF) process allows overcoming two key limitations of the conventional chemical method [11-13]: (i) it ensures the continuous regeneration of Fe^{2+} through cathodic reduction of Fe^{3+}, thus requiring a much lower amount of catalyst to perform the treatment, and (ii) it avoids the handling, storage and transportation of H_2O_2 produced industrially, since this reagent can be electrosynthesized on site through Reaction (1) by using appropriate cathode materials.

$$O_{2(g)} + 2H^+ + 2e^- \rightarrow H_2O_2 \qquad (1)$$

Electrocatalytic H_2O_2 generation is becoming a hot topic because the combination of electrochemistry with new catalysts enables a more eco-friendly and less energy-intensive production of this commodity [14,15]. Several prospective electrocatalysts have been

63   developed, with noble metals and metal alloys like Pd-Au, Pt-Hg and Pt/Pd-Hg as particularly

64   prominent options [14,16,17]. Non-precious Co-based particles are very active promoters of

65   Reaction (1) as well, at smaller cost [18]. Unfortunately, none of these catalysts is viable for

66   large-scale water treatment due to their high cost and toxicity, which has fostered the

67   investigation on inexpensive carbonaceous materials [14,19,20]. Unmodified carbon-based

68   catalysts exhibit appealing characteristics as cathodes, such as non-toxicity and high stability,

69   conductivity and durability. H_2O_2 production with such inexpensive materials is particularly

70   interesting for developing small- or medium-size decentralized units where the chemical is

71   generated on demand [21]. This can be achieved using graphite felt, reticulated vitreous

72   carbon, activated carbon fiber or carbon nanotubes as cathode, completely immersed into the

73   solution to generate H_2O_2 from dissolved O_2 [22-24]. However, much greater H_2O_2

74   concentrations are attained upon implementation of an air-chamber in the electrochemical

75   reactor, since it allows continuous air-feeding through a hydrophobized carbon-based gas-

76   diffusion electrode (GDE) [15,18,25-28]. Worth noting, the vast majority of studies on

77   Fenton-based electrochemical AOPs (EAOPs) reporting data on H_2O_2 production at GDE

78   have been carried out either at laboratory scale or in small pre-pilot plants of 2.5 L [29] and 5

79   L [30,31]. Only one work reported the use of a bigger plant with 25 L capacity, but it was

80   mainly focused on aniline degradation [32].

81   Undivided electrochemical cells are preferred to perform all these studies on water

82   treatment because the use of a separator would increase the cell voltage and hence, the energy

83   consumption. In addition, in such cells, the combination of carbonaceous cathodes with

84   electrocatalytic materials that promote the anodic production of heterogeneous hydroxyl

85   radical enhances the performance of EF process. Boron-doped diamond (BDD) thin film on Si

86   substrate is the best anode to oxidize H_2O to physisorbed $^{\bullet}OH$ via Reaction (2) [11,13,33],

owing to its large overpotential for O_2 evolution. However, Ti and Nb are more suitable for plant-scale applications due to their much higher mechanical and chemical resistance.

$$BDD + H_2O \rightarrow BDD(^\bullet OH) + H^+ + e^- \qquad (2)$$

The best performance among Fenton-based EAOPs for SOCs degradation is attained upon continuous irradiation of the treated solution with UV/Vis light. This is feasible employing a UVA lamp in photoelectro-Fenton (PEF) process [11,13], since it promotes: (i) a high regeneration rate of Fe^{2+}, with concomitant production of homogeneous $^\bullet OH$, from photoreduction of the main Fe(III) species at pH ~ 3.0 (Reaction (3)), (ii) the photodegradation of Fe(III)-carboxylate complexes formed as intermediates (Reaction (4)), and (iii) the direct photolysis of some pollutants and/or their oxidation by-products [11,34].

$$[Fe(OH)]^{2+} + h\nu \rightarrow Fe^{2+} + {}^\bullet OH \qquad (3)$$

$$[Fe(OOCR)]^{2+} + h\nu \rightarrow Fe^{2+} + CO_2 + R^\bullet \qquad (4)$$
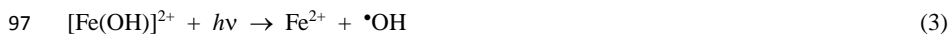
In order to achieve the synergy between electrocatalytic and photolytic reactions at an affordable cost, UVA lamps have been lately replaced by direct sunlight irradiation, yielding the promising solar PEF (SPEF) process. Its great oxidation capability arises from: (i) the higher UV photon flux from sun if the solar collector design is adapted to the photoreactor, which upgrades the $^\bullet OH$ production, along with (ii) the additional illumination within the visible range ($\lambda > 400$ nm), promoting Reaction (3) (also active in the visible range) and accelerating the photolysis of refractory Fe(III)-carboxylate complexes (Reaction (4)) [34]. Very good degradation results by SPEF with GDE were obtained using a recirculation small pilot plant of 2.5-L capacity equipped with a flat-plate photoreactor [35-37], also employed to treat pesticides like mecoprop [35], diuron [38] or tebuthiuron and ametryn [39]. Replacement by a more efficient photoreactor based on compound parabolic collectors (CPC) could increase the efficiency of SPEF due to the greater photon flux supply to the solution. At

111 present, CPC is the most popular photoreactor, as confirmed by its integration in most of the

112 SPEF units for treating 2.2 L [40], 6 L [41], 8 L [42] and up to 10 L [43-48], which is the

113 largest volume investigated so far.

114   Based on the excellent performance of SPEF at limited scale, a larger pilot plant has been

115 developed for the treatment of SOCs by EAOPs with H_2O_2 electrogeneration. The system,

116 with capacity to treat up to 100 L, consists of four undivided Nb-BDD/GDE filter-press cells

117 coupled with a solar CPC, and has been installed and tested at Plataforma Solar de Almería

118 (PSA), the largest European facility to test solar technologies. As a first step toward the

119 treatment of real wastewater, this work is focused on the optimization of pilot plant main

120 operation variables for the electrocatalytic H_2O_2 production, including current density (j),

121 solution pH, liquid flow rate, air flow rate and electrolyte concentration. This was made with

122 the aid of central composite design (CCD) coupled to response surface methodology (RSM).

123 The plant was further validated by performing degradation trials under optimum conditions

124 using a mixture of fungicide PYR and insecticide MET spiked into conductive water at high

125 concentrations to simulate real agricultural wastewater. Note that these pesticides have only

126 been studied before by AOPs like solar TiO_2 photocatalysis and solar photo-Fenton at pilot

127 scale [6] and EF at lab scale [8].

128 **2. Materials and methods**

129 *2.1. Chemicals*

130   Heptahydrated ferrous sulfate (Sigma-Aldrich) used as catalyst and anhydrous sodium

131 sulfate (Fluka) employed as background electrolyte were of analytical grade. PYR (IQV,

132 AgroEvo, 98% purity) and MET (Aragonesas Agro, 99.5% purity) were of reagent grade and

133 used without further purification. Mixtures of the two pesticides were prepared with deionized

134 water (conductivity < 10 µS cm^{-1}, dissolved organic carbon (DOC) < 0.5 mg L^{-1}) and the

135 electrolyte, and their pH was adjusted with analytical grade sulfuric acid (J.T. Baker). Organic

136 solvents and other chemicals employed for HPLC analysis of the pesticides were of analytical

137 grade from Sigma-Aldrich.

138 *2.2. Pilot plant*

139   Images of the filter-press type electrochemical cells and the CPC photoreactor, along with

140 a schematic diagram of the pilot plant, are shown in Fig. 1. The plant consisted of four plate-

141 and-frame electrochemical reactors (Electro MP-Cells from ElectroCell) coupled to a

142 purpose-made solar CPC. Each cell contained an anode made of BDD thin film deposited on a

143 niobium mesh (Nb-BDD) and a carbon-polytetrafluoroethylene (PTFE) GDE as the cathode,

144 both with 0.01 m^2 effective area. The CPC photoreactor had a total illuminated area of 2 m^2,

145 corresponding to an irradiated volume of 23 L. It was comprised of 10 borosilicate glass tubes

146 (150 cm length $\times$ 4.5 cm inner diameter) mounted in an aluminum frame on a platform tilted

147 37º (PSA, 37ºN, 2.4ºW). The working volume was 25 L to carry out the optimization of H_2O_2

148 electrogeneration, and 75 L to perform the degradation experiments. The unit was equipped

149 with two magnetic drive pumps (PAN World, 0.75 kW), one for pumping the solution from

150 the feed tank (maximum capacity of 100 L) to the electrochemical cells, and the other for the

151 liquid recirculation to and from the CPC. The GDE was fed with compressed air (ABAC air

152 compressor, 1.5 kW) at a pressure and flow rate regulated with a back-pressure gauge and a

153 flowmeter, respectively, in order to avoid the flooding of the air chamber. The experiments

154 were made at constant *j* using a Delta Electronika power supply (limited to 70 V and 22 A).

155   Global ultraviolet solar radiation (UV_G) was measured using a radiometer (Kipp &

156 Zonen, model CUV 3) mounted on a platform tilted 37°, the same angle as the photoreactor,

157 which provided data in terms of incident irradiance (W_{UV} m^{-2}). This informs about the energy

158 reaching any surface in the same position with regard to the sun. Eq. (5) allows combining the

159 data from trials performed in different days, thus enabling comparison with results obtained in

160 other photocatalytic experiments [49].

$$Q_{UV,n} = Q_{UV,n-1} + \Delta t_n \cdot \overline{UV}_{G,n} \cdot A_r \cdot V_T \qquad (5)$$

161 where Q_{UV} is the accumulated UV energy per unit of volume (kJ L^{-1}), $\overline{UV}_{G,n}$ (in W m^{-2}) is the

162 average UV radiation measured during Δt_n ($= t_n - t_{n-1}$), A_r is the irradiated surface area (2 m^2)

163 and V_T is the total volume treated in the pilot plant.

2.3. Experimental design

165 Experimental design by RSM was employed to optimize the in situ electrogeneration of

166 H_2O_2. Trials were performed with one of the four identical electrochemical cells of the pilot,

167 assuming that the resulting optimum conditions would be also valid for the other three cells.

168 Two optimization criteria were considered: (a) maximization of the concentration of the

169 produced H_2O_2, and (b) maximization of the current efficiency (CE, in percentage), defined as

170 the ratio between the electricity consumed by the electrode reaction of interest and the total

171 electricity supplied. CE can be calculated via Eq. (6), where *n* represents the stoichiometric

172 number of electrons transferred in Reaction (1), *F* is the Faraday constant (96,487 C mol^{-1}),

173 [H_2O_2] the concentration of H_2O_2 accumulated in bulk solution (mg L^{-1}), V_T the volume of the

174 treated solution (L), $M(H_2O_2)$ the molecular weight of H_2O_2 (34 g mol^{-1}), and Q the charge

175 consumed during the electrolysis (C).

176 $\% \, CE = \dfrac{nF[H_2O_2]V_T}{1000 \, M(H_2O_2)Q} \times 100 \qquad (6)$

177 RSM was first used to assess the relationship between response (H_2O_2 concentration or %

178 CE) and two independent variables, namely the solution pH (factor A) and *j* (factor B), as

179 well as to optimize the relevant conditions in order to predict the best value of responses.

180 CCD, the most widely used approach of RSM and, more specifically, a face centered

181 composite (FCC) design, was employed to determine the effect of the two variables. Design

Expert® v.7.0.0 software (Stat-Ease Inc., USA) was used. Three levels between -1 and +1 were established for the two independent variables (Table 1). Ranges were chosen based on preliminary experiments (data not shown here), background knowledge, and some constraints arising from the cathodic H_2O_2 electrogeneration and the nature of the electrode materials. For example, the production of H_2O_2 is favored at acidic pH (Reaction (2)), whereas the use of GDE and BDD anode limits the operation cell voltage to less than 25 V to prevent surface damage, which would cause the loss of electrocatalytic properties, and keep a reasonable CE [50]. This means that maximum current that can be applied is 10 A ($j = 100$ mA cm^{-2}).

For the CCD, a 2^3 full factorial design with 3 replicates at the center point (resulting in 19 experiments) was used to determine the optimum values of independent variables. These experiments were carried out by recirculating synthetic solutions of 50 mM Na_2SO_4 at a liquid flow rate of 4.4 L min^{-1}, and they were randomly performed to minimize the effect of systematic errors. Analysis of variance (ANOVA) of the data was performed to identify significant values (p-value < 0.05). The quality of the fit of polynomial model was expressed by the value of correlation coefficient (R^2). The main indicators demonstrating the significance and adequacy of the used model include the model F-value (Fisher variation ratio), probability value (Prob $>$ F), and adequate precision. The optimal region of the independent variables was determined by plotting three-dimensional response surfaces of the independent and dependent variables. Additionally, numerical optimization of the independent variables was carried out using the same software.

A second set of experiments was carried out aiming to assess the effect of electrolyte concentration as well as liquid and air flow rates, under the optimum pH and j conditions. The best operation conditions were finally applied to degrade mixtures of pesticides, in the absence or presence of iron catalyst. In SPEF, the pesticide solution was irradiated when circulating through the CPC photoreactor.

2.4. Instruments and analytical methods

208   The concentration of H_2O_2 accumulated during the electrolysis was determined by adding

209 Ti(IV) oxysulfate to the sample and measuring the absorbance at 410 nm, according to DIN

210 38409 H15. Iron concentration was measured by using 1,10-phenanthroline, following ISO

211 6332. In both cases, a Unicam UV/Vis UV2 spectrophotometer was employed. Dissolved

212 organic carbon (DOC) was measured after sample filtration through a 0.22 μm Nylon filter,

213 on a Shimadzu TOC-VCSN analyzer. The degradation rate of the two pesticides was

214 monitored on a UPLC/UV Agilent Technologies Series 1200, equipped with a C-18

215 ZORBAX XDB C-18 analytical column. The column was kept at 30 ºC and the injection

216 volume was 50 μL. A linear gradient profile with water and acetonitrile (ACN) eluted at a

217 flow rate of 1 mL min^{-1} was established as follows: 0-4 min, isocratic at 85/15 (v/v)

218 H_2O/ACN; 4-8 min, gradient from 85/15 to 20/80 (v/v); 8-15 min, isocratic at 85/15 (v/v). Re-

219 equilibration time was 3 min. The UV signals for MET and PYR were monitored at the

220 wavelength of their maximum absorption, 230 nm and 270 nm, respectively. For UPLC

221 analyses, 9 mL of sample were filtered through a 0.22 μm PTFE syringe filter. Then, it was

222 washed with 1 mL of UPLC grade ACN to extract any compound adsorbed on the filter. The

223 pH of the treated solution was monitored by means of a Crison 25 pH-meter.

224 **3. Results and discussion**

225 *3.1. Influence of independent experimental variables on the in situ H_2O_2 electrogeneration*

226   The results obtained from the experimental design matrix including the two independent

227 variables (pH, *j*) are shown in Table 2. The responses (H_2O_2 concentration and % CE) are

228 presented at two electrolysis times, 5 and 30 min, corresponding to approximately one and

229 five circulations of the initial feed solution volume (25 L) through the electrochemical cell,

230 respectively. The average values of the two responses at 30 min are illustrated in Fig. 2a,

whereas the changes in H_2O_2 mass production rate over the electrolysis time are depicted at constant pH = 3.0 (Fig. 2b) or j = 100 mA cm^{-2} (Fig. 2c).

As expected, a higher accumulation of H_2O_2 was found as the electrolyses were prolonged, although this occurred in concomitance with current efficiency decrease (Table 2). This is also confirmed from the profiles of the H_2O_2 production rates with time, since the highest values were attained at the beginning of the electrolyses until quasi-steady values were observed at longer times, regardless of the j (Fig. 2b) or the pH (Fig. 2c) studied. According to Eq. (6), the gradual lower efficiency with electrolysis time is related to the reduced $[H_2O_2]/Q$ ratio as a result of nonlinear increase of the accumulated H_2O_2. This kind of behavior can be partly explained by the use of batch operation mode, since the H_2O_2 production rate at the air-diffusion cathode from Reaction (1) becomes equal to its decomposition rate by parasitic reactions that can take place in the cell. For example, the continuous recirculation of H_2O_2 accumulated in the solution may promote its electrochemical reduction at the cathode surface (Reaction (8)) and, to much lesser extent, its spontaneous disproportion in the bulk (Reaction (9)) [11].

$$H_2O_2 + 2H^+ + 2e^- \rightarrow 2H_2O \tag{8}$$

$$H_2O_2 \rightarrow \tfrac{1}{2} O_{2(g)} + H_2O \tag{9}$$

Furthermore, considering that an undivided electrochemical reactor is employed, other additional parasitic reactions occur, as for example the oxidation of H_2O_2 to O_2 at the Nb-BDD anode surface via $HO_2^\bullet$ as an intermediate, according to the following reactions:

$$H_2O_2 \rightarrow HO_2^\bullet + H^+ + e^- \tag{10}$$

$$HO_2^\bullet \rightarrow O_{2(g)} + H^+ + e^- \tag{11}$$

In addition, it is worth mentioning that H_2O_2 decomposition is promoted as the solution pH becomes more alkaline, according to the following reaction:

$$H_2O_2 + OH^- \rightarrow H_2O + HO_2^- \tag{12}$$

256   As a consequence of these undesired reactions, the accumulated H_2O_2 concentration is

257   always below the theoretical maximum. As explained in the Introduction, undivided reactors

258   are the best choice for water treatment, but divided ones should be employed for industrial

259   electrochemical H_2O_2 production. Note that similar trends for H_2O_2 accumulation have been

260   reported by Brillas and co-workers, as shown during the electrolysis of Na_2SO_4 solutions in a

261   similar batch filter-press BDD/GDE reactor at j values between 50 and 150 mA cm^{-2} [29].

262   In addition, Fig. 2b and 2c show that the maximum H_2O_2 production was achieved at 100

263   mA cm^{-2} and pH 3.0. This agrees with the fact that a higher electron and proton supply

264   promotes a faster O_2 reduction from Reaction (1).

265   *3.2. Validation of the correlation models*

266   With the aid of Design Expert software, the models that best correlated the responses and

267   the independent variables shown in Table 2 were:

268   (i)   Quadratic model:

269    $$[H_2O_2] = 2.19 - 0.31 \cdot pH + 0.81 \cdot j - 0.05 \cdot pH \cdot j + 0.15 \cdot pH^2 - 2.42 \times 10^{-3} \cdot j^2 \qquad (12)$$

270   (ii)   Two-factor interaction model (2FI):

271    $$\% \ CE = 61.68 - 0.43 \cdot pH - 0.18 \cdot j - 0.0275 \cdot pH \cdot j \qquad (13)$$

272   Both models were validated by the analysis of variances (ANOVA), and the results are

273   summarized in Table 3. The statistical significance was assessed by means of Fisher's test.

274   The F-values calculated for the lack of fit of the quadratic and the 2FI models were 30.44 and

275   60.89, respectively, suggesting that they are satisfactory. Similar conclusions can be drawn

276   from the low probability values (p-value) at a 95% confidence level (< 0.0001) for both

277   models. The statistical significance of the two models is also verified from Fig. 3, since the

278   actual values of the accumulated H_2O_2 concentration and current efficiency are randomly

279   distributed around the mean of predicted values. Moreover, good linear correlations between

the predicted and observed values for H_2O_2 concentration and % CE, with corresponding R^2 values of 0.932 and 0.924, were obtained.

According to the ANOVA analysis (Table 3), the effects of the independent variables (A-pH, B-j) were obvious and the effective order was j > initial pH, whereas the interaction of the two variables (AB) was not obvious (p-value > 0.1). This can also be deduced from Fig. 2b and 2c, which show that the H_2O_2 production is more substantially affected by j (Fig. 2b) rather than by solution pH, with the latter showing only a slight superiority at pH 3.0 as compared to neutral pH (Fig. 2c). This is important, since the adjustment of pH when treating wastewater complicates the process and increases the water salinity and the operation cost (for acidification and subsequent neutralization).

3.3. Optimization by response surface methodology

To better assess the effect of pH and j on H_2O_2 production and current efficiency and identify their optimum values, 3D response surfaces and contour maps were developed with the aid of Design Expert software. The response surface plot shown in Fig. 4 implies that the generation of H_2O_2 increases with j at acidic pH values. On the other hand, the current efficiency (Fig. 5) decreases as j is raised, regardless of the initial pH of the electrolyte solution. As explained above, this is attributed to the batch operation mode in an undivided cell configuration, which promotes the activation of detrimental side reactions. Four sets of optimum pH and j values were proposed by the statistical software (Table 4), yielding maximum H_2O_2 production and current efficiency. Among the four solutions proposed, solution number 1, requiring electrolyte pH = 3.0 and j = 73.66 mA cm^{-2} (~74.0), was selected as the optimum one. Under these conditions, a set of experiments was conducted aiming to validate the two correlation models (Eq. (12) and (13)) and to investigate the effect of other operation conditions like liquid and air flow rates, as well as electrolyte concentration. The main goal was to fully optimize the electrocatalytic H_2O_2 production at plant scale, eventually

305   yielding the most effective (highest H_2O_2 production rate), efficient (maximum CE

306   percentage) and profitable (lowest energy consumption) process at large scale.

307   The results of two replicate experiments under the aforementioned optimum conditions

308   are summarized in Table 5. The relative errors were below 5% for both, H_2O_2 generation and

309   % CE (3.69% and 4.38%, respectively), demonstrating the excellent fitting of the

310   experimental results (actual values) with those predicted by the two models.

311   *3.3.1. Effect of liquid flow rate*

312   The feed flow rate is closely related to the hydraulic residence time (HRT) of the treated

313   solution within the electrochemical cell. This is of great significance under continuous

314   operation mode, where the feed solution is continuously treated and discharged. For batch

315   operation, as is the case of the experiments carried out in this work, the recirculation flow rate

316   does not necessarily match the HRT, but it rather affects the mixing and may create turbulent

317   flow within the electrochemical cell. This, in turn, may intensify the mass transport induced

318   by the higher local concentration of molecular oxygen dissolved in the aqueous phase. Indeed,

319   when the flow rate was doubled (from 2.8 to 5.6 L min^{-1}), H_2O_2 production was gradually

320   greater at each given time (Fig. 6b), finally increasing by 28.8% at 30 min (Fig. 6a, [H_2O_2] in

321   mg min^{-1}). Current efficiency also increased in the same proportion, as a result of the higher

322   H_2O_2 generation at similar charge consumption (note that energy consumption varied between

323   1.97 and 2.00 kWh m^{-3} for all pilot runs) (Fig. 6a).

324   *3.3.2. Effect of air flow rate*

325   Large feeding of air or pure O_2 to the air chamber is often needed to counterbalance the

326   existing pressure on the wet face of the GDE, thereby avoiding flooding that would stop the

327   H_2O_2 production. If correctly adjusted, an increase in air flow rate may upgrade the H_2O_2

328   accumulation. As found for the pilot plant studied in this work, a rise in the air flow rate from

329   2.5 and 5 L min^{-1} to 10 L min^{-1}, resulted in an enhanced H_2O_2 production by 23.1% and

330   15.6% at 30 min, respectively (Fig. 7a and 7b). Moreover, the kinetics of H_2O_2 production

331   was faster at the maximum air flow rate of 10 L min^{-1} (Fig. 7b), with no negative effect on the

332   corresponding energy consumption, which was similar at all air flow rates examined. This is

333   interesting, since one might presume that an excessive air feeding could generate too many

334   bubbles within the electrochemical reactor, thereby increasing the ohmic drop and also

335   affecting the stability of the liquid flow rate, which did not occur.

336   Based on these results, as well as on the better performance of the plant at high

337   electrolyte flow rates, it can be concluded that the combined increase of air and liquid flow

338   rates may effectively enhance the fraction of oxygen consumed for H_2O_2 production

339   (Reaction (1)) over the total amount of air fed. Indeed, under the optimum operation

340   conditions, namely 50 mM Na_2SO_4 solution at pH 3.0 treated at 74 mA cm^{-2}, with liquid flow

341   rate of 5.6 L min^{-1} and air flow rate of 10 L min^{-1}, the highest H_2O_2 mass production rate and

342   current efficiency were obtained. In the first 5 min of electrolysis, these conditions led to

343   H_2O_2 production with a mass rate of 64.9 mg min^{-1}, 89.3% current efficiency and energy

344   consumption of 0.4 kWh m^{-3}. These values are among the best achieved with similar system

345   configurations. For example, Flox et al. [29] reported a production rate of ca. 23 mg min^{-1} at

346   30 min in 50 mM Na_2SO_4 at pH 3.0, 100 mA cm^{-2} and liquid flow rate of 3 L min^{-1}, whereas

347   Fig. 7a shows a higher H_2O_2 electrogeneration rate of 32 mg min^{-1} at that time.

348   *3.3.3. Effect of electrolyte concentration*

349   Considering the rather small electrode gap (6 mm) between the anode and cathode in the

350   electrochemical cell, it was assumed that the solution conductivity would not significantly

351   affect the production of H_2O_2. Therefore, a set of experiments was made to determine the

352   possible influence of electrolyte concentration. It was observed that, within the range of 25-75

353   mM of Na_2SO_4, which is equal to a solution conductivity range of 4.6 to 12.3 mS cm^{-1}, the

354   accumulation of H_2O_2 was quite analogous, being only slightly higher in the case of 50 mM

355 (Fig. 8). However, a rather substantial effect is observed regarding the energy consumption,

356 since a higher conductivity led to a gradually lower consumption; i.e. 3.24, 2.00 and 1.61

357 kWh m^{-3} at 25, 50 and 75 mM Na$_2$SO$_4$, respectively. This was expected, since the increase of

358 electrolyte concentration causes a reduction of the ohmic resistance in the bulk solution, and

359 accelerates the electron transfer, thus decreasing the overall charge consumption. From these

360 findings, it can be concluded that the system would be more efficient at higher water

361 conductivity. Therefore, future industrial application of this technology should focus on high

362 conductivity wastewater or be coupled with membrane technologies for treating membrane

363 concentrates.

364 *3.4. Treatment of a mixture of pesticides*

365 After the optimum operation conditions were determined for attaining the best balance

366 between H$_2$O$_2$ production and current efficiency, the plant performance was validated by

367 carrying out several tests to assess its capability to degrade a mixture of two model SOCs,

368 namely PYR and MET, which were treated by sun-assisted AOPs like solar photo-Fenton

369 [6,51]. All the assays were made with 75 L of mixtures of both pesticides in water with 50

370 mM Na$_2$SO$_4$ under optimized conditions: pH 3.0, 74 mA cm^{-2} and air flow rate of 10 L min^{-1}.

371 First, a mixture containing 50 mg L^{-1} PYR and 90 mg L^{-1} MET (i.e., 71 mg L^{-1} DOC) was

372 treated by EO with electrogenerated H$_2$O$_2$. The influence of liquid flow rate (2.8, 4.4 and 5.6

373 L min^{-1}) was investigated, aiming to promote a larger oxidation of both organic contaminants

374 either by increasing the HRT (at a lower flow rate) or by enhancing the mass transport of

375 pollutants to the anode surface (at a higher flow rate). However, no significant effect of this

376 parameter was found, which suggests that the amount of BDD($^{\bullet}$OH) produced via Reaction

377 (2) at 74 mA cm^{-2} was high enough to react with both pesticides regardless of the

378 hydrodynamic conditions (within the studied range). Fig. 9a and 9b depict the normalized

379 decays of PYR and MET concentrations at a liquid flow rate of 5.6 L min^{-1}, respectively. As

380 can be seen, the degradation by EO-H_2O_2 was very slow, only attaining 20% and 30% of PYR

381 and MET removal after 120 min. The larger degradation of MET could be explained by the

382 greater electrocatalytic behavior of BDD with this pesticide as a result of a more favorable

383 adsorption on its surface, thus reacting more quickly with physisorbed BDD($^\bullet$OH). At the end

384 of the electrolysis, almost no mineralization was achieved in EO process, in agreement with

385 the refractory nature of typical reaction by-products like carboxylic acids [10-13]. In all these

386 trials, the energy consumption was around 10 kWh m^{-3}.

387   The same pesticides mixture was treated by EF, using the optimized parameters with

388 liquid flow rate of 5.6 L min^{-1}, in the presence of different amounts of Fe^{2+} as catalyst (not

389 shown). After 120 min, a higher degradation percentage was reached for both pesticides, with

390 up to 35% and 40% for PYR and MET, respectively. This demonstrates that the H_2O_2

391 produced under optimized conditions reacted with added Fe^{2+} according to Fenton's reaction,

392 yielding homogeneous $^\bullet$OH that enhanced the degradation because this radical acted

393 concomitantly with BDD($^\bullet$OH). The former was confined into the reactor, whereas the latter

394 radical was transported throughout the whole volume. In contrast, DOC abatement only

395 attained 8% as maximum, which agrees with the high stability of Fe(III)-carboxylate

396 complexes formed as intermediates [11]. Worth mentioning, a much larger mineralization was

397 achieved working with a pesticide mixture that accounted for 20 mg L^{-1} DOC, using 1.0 mM

398 Fe^{2+}. In this case, 32% DOC removal was attained at 120 min. It is also important to note that

399 the Fe^{2+} concentration remained almost constant during all these EF trials, which confirms the

400 capability of the cathode to regenerate it from Fe(III) reduction.

401   Finally, the mixtures with 71 mg L^{-1} DOC were comparatively treated by SPEF using the

402 best Fe^{2+} concentration (i.e., 0.5mM). In these experiments, required accumulated UV energy,

403 $Q_{UV,}$ was 7.1 kJ L^{-1}. As it can be observed in Fig. 9, 55% and 50% removal of PYR and MET

404 was reached in only 5 min, which confirms the fast Fe^{2+} photoregeneration with additional

405 •OH production from Reaction (3). At longer time, the degradation was much slower, but

406 ended in 77% and 70% removal, respectively, at 120 min. This is a much better performance

407 as compared to EO and EF, which was further confirmed by DOC abatements higher than

408 15%, in agreement with the powerful action of UV/Vis photons on Fe(III)-carboxylate

409 complexes according to Reaction (4).

410 **4. Conclusions**

411   The successful performance of the largest SPEF pilot plant existing to date has been

412 demonstrated in this work. The core of the plant, the filter-press electrochemical reactor, is

413 comprised of a Nb-BDD anode and a GDE as cathode. Optimization of main operation

414 parameters has been carried out according to a thorough experimental design, in order to

415 maximize the electrocatalytic H_2O_2 production with a high current efficiency. Optimum

416 values obtained for the key parameters were: pH 3.0, 74 mA cm^{-2}, liquid flow rate of 5.6 L

417 min^{-1} and air flow rate of 10 L min^{-1}. Their application yielded a mass rate of up to 64.9 mg

418 H_2O_2 min^{-1}, current efficiency of 89.3% and energy consumption of 0.4 kWh m^{-3} during the

419 first minutes. The SPEF treatment of 75 L of pesticides mixtures allowed the removal of more

420 than 50% of each pesticide in only 5 min, where upon further degradation as well as

421 mineralization of by-products and their Fe(III) complexes became much slower but always

422 superior to EO and EF treatments. Further optimization of the SPEF process for treating

423 different kind of wastewater in the integrated pilot system is in progress.

430 **References**

431 [1] R. Loos, B.M. Gawlik, G. Locoro, E. Rimaviciute, S. Contini, G. Bidoglio, Environ.

432 Pollut. 157 (2009) 561-568.

433 [2] The NORMAN Network, http://www.norman-network.net/?q=Home, 2012 (accessed

434 15 May 2018).

435 [3] J.-Q. Jiang, Z. Zhou, V.K. Sharma, Microchem. J. 110 (2013) 292-300.

436 [4] B. Petrie, R. Barden, B. Kasprzyk-Hordern, Water Res. 72 (2015) 3-27.

437 [5] C. Postigo, D. Barceló, Sci. Total Environ. 503-504 (2015) 32-47.

438 [6] I. Oller, S. Malato, J.A. Sánchez-Pérez, M.I. Maldonado, R. Gassó, Catal. Today 129

439 (2007) 69-78.

440 [7] D.J.E. Costa, J.C.S. Santos, F.A.C. Sanches-Brandão, W.F. Ribeiro, G.R. Salazar-

441 Banda, M.C.U. Araujo, J. Electroanal. Chem. 789 (2017) 100-107.

442 [8] M. Popescu, C. Sandu, E. Rosales, M. Pazos, G. Lazar, M.A. Sanromán, J. Electroanal.

443 Chem. 808 (2018) 455-463.

444 [9] C. Comninellis, A. Kapałka, S. Malato, S.A. Parsons, I. Poulios, D. Mantzavinos, J.

445 Chem. Technol. Biotechnol. 83 (2008) 769-776.

446 [10] M.A. Oturan, J.-J. Aaron, Crit. Rev. Environ. Sci. Technol. 44 (2014) 2577-2641.

447 [11] E. Brillas, I. Sirés, M.A. Oturan, Chem. Rev. 109 (2009) 6570-6631.

448 [12] L. Feng, E.D. van Hullebusch, M.A. Rodrigo, G. Esposito, M.A. Oturan, Chem. Eng. J.

449 228 (2013) 944–964.

450 [13] C.A. Martínez-Huitle, M.A. Rodrigo, I. Sirés, O. Scialdone, Chem. Rev. 115 (2015)

451 13362-13407.

452   [14]   S. Chen, Z. Chen, S. Siahrostami, T.R. Kim, D. Nordlund, D. Sokaras, S. Nowak,
453   J.W.F. To, D. Higgins, R. Sinclair, J.K. Nørskov, T.F. Jaramillo, Z. Bao, ACS Sustain.
454   Chem. Eng. 6 (2018) 311-317.

455   [15]   T. Pérez, G. Coria, I. Sirés, J.L. Nava, A.R. Uribe, J. Electroanal. Chem. 812 (2018) 54-
456   58.

457   [16]   S. Siahrostami, A. Verdaguer-Casadevall, M. Karamad, D. Deiana, P. Malacrida, B.
458   Wickman, M. Escudero-Escribano, E.A. Paoli, R. Frydendal, T.W. Hansen, Ib
459   Chorkendorff, I.E.L. Stephens, J. Rossmeisl, Nature Mater. 12 (2013) 1137-1143.

460   [17]   E. Pizzutilo, O. Kasian, C.H. Choi, S. Cherevko, G.J. Hutchings, K.J.J. Mayrhofer, S.J.
461   Freakley, Chem. Phys. Lett. 683 (2017) 436-442.

462   [18]   C. Ridruejo, F. Alcaide, G. Álvarez, E. Brillas, I. Sirés, J. Electroanal. Chem. 808
463   (2018) 364-371.

464   [19]   G.-L. Chai, Z. Hou, T. Ikeda, K. Terakura, J. Phys. Chem. C 121 (2017) 14524-14533.

465   [20]   V. Čolić, S. Yang, Z. Révay, I.E.L. Stephens, Ib Chorkendorff, Electrochim. Acta 272
466   (2018) 192-202.

467   [21]   S. Yang, A. Verdaguer-Casadevall, L. Arnarson, L. Silvioli, V. Čolić, R. Frydendal, J.
468   Rossmeisl, Ib Chorkendorff, I.E.L. Stephens, ACS Catal. 8 (2018) 4064-4081.

469   [22]   A. Dirany, I. Sirés, N. Oturan, A. Özcan, M.A. Oturan, Environ. Sci. Technol. 46
470   (2012) 4074-4082.

471   [23]   M. Panizza, A. Dirany, I. Sirés, M. Haidar, N. Oturan, M.A. Oturan, J. Appl.
472   Electrochem. 44 (2014) 1327-1335.

473   [24]   G. Coria, T. Pérez, I. Sirés, J.L. Nava, J. Electroanal. Chem. 757 (2015) 225-229.

474   [25]   K.V. Plakas, S.D. Sklari, D.A. Yiankakis, G.Th. Sideropoulos, V.T. Zaspalis, A.J.
475   Karabelas, Water Res. 91 (2016) 183-194.

476   [26] A. Galia, S. Lanzalaco, M.A. Sabatino, C. Dispenza, O. Scialdone, I. Sirés,
477   Electrochem. Commun. 62 (2016) 64-68.

478   [27] Z.G. Aguilar, E. Brillas, M. Salazar, J.L. Nava, I. Sirés, Appl. Catal. B: Environ. 206
479   (2017) 44-52.

480   [28] S. Lanzalaco, I. Sirés, M.A. Sabatino, C. Dispenza, O. Scialdone, A. Galia,
481   Electrochim. Acta 246 (2017) 812-822.

482   [29] C. Flox, J.A. Garrido, R.M. Rodríguez, P.-L. Cabot, F. Centellas, C. Arias, E. Brillas,
483   Catal. Today 129 (2007) 29-36.

484   [30] G.R. Agladze, G.S. Tsurtsumia, B.-I. Jung, J.-S. Kim, G. Gorelishvili, J. Appl.
485   Electrochem. 37 (2007) 375-383.

486   [31] M. Giomo, A. Buso, P. Fier, G. Sandonà, B. Boye, G. Farnia, Electrochim. Acta 54
487   (2008) 808-815.

488   [32] E. Brillas, J. Casado, Chemosphere 47 (2002) 241-248.

489   [33] B. Chaplin, Environ. Sci.: Processes Impacts 16 (2014) 1182-1203.

490   [34] E. Brillas, J. Braz. Chem. Soc. 25 (2014) 393-417.

491   [35] C. Flox, P.L. Cabot, F. Centellas, J.A. Garrido, R.M. Rodríguez, C. Arias, E. Brillas,
492   Appl. Catal. B: Environ. 75 (2007) 17-28.

493   [36] A. Thiam, I. Sirés, E. Brillas, Water Res. 81 (2015) 178-187.

494   [37] J.R. Steter, E. Brillas, I. Sirés, Appl. Catal. B: Environ. 224 (2018) 410-418.

495   [38] A.R.F. Pipi, I. Sirés, A.R. De Andrade, E. Brillas, Chemosphere 109 (2014) 49-55.

496   [39] F. Gozzi, I. Sirés, A. Thiam, S.C. de Oliveira, A. Machulek Jr., E. Brillas, Chem. Eng. J.
497   310 (2017) 503-513.

498   [40] F.C. Moreira, J. Soler, A. Fonseca, I. Saraiva, R.A.R. Boaventura, E. Brillas, V.J.P.
499   Vilar, Appl. Catal. B: Environ. 182 (2016) 161-171.

500   [41] G. Coria, T. Pérez, I. Sirés, E. Brillas, J.L. Nava, Chemosphere 198 (2018) 174-181.

501 [42] C. Espinoza, J. Romero, L. Villegas, L. Cornejo-Ponce, R. Salazar, J. Hazard. Mater.
502   319 (2016) 24-33.

503 [43] L.C. Almeida, S. Garcia-Segura, N. Bocchi, E. Brillas, Appl. Catal. B: Environ. 103
504   (2011) 21-30.

505 [44] E. Isarain-Chávez, R.M. Rodríguez, P.L. Cabot, F. Centellas, C. Arias, J.A. Garrido, E.
506   Brillas, Water Res. 45 (2011) 4119-4130.

507 [45] S. Garcia-Segura, E. Brillas, Electrochim. Acta 140 (2014) 384-395.

508 [46] V. S. Antonin, S. Garcia-Segura, M.C. Santos, E. Brillas, J. Electroanal. Chem. 747
509   (2015) 1-11.

510 [47] S. Garcia-Segura, E. Brillas, Appl. Catal. B: Environ. 181 (2016) 681-691.

511 [48] T. Pérez, I. Sirés, E. Brillas, J.L. Nava, Electrochim. Acta 228 (2017) 45-56.

512 [49] S. Malato, J. Blanco, A. Campos, J. Cáceres, C. Guillard, J.M. Herrmann, A.R.
513   Fernández-Alba, Appl. Catal. B: Environ. 42 (2003) 349-357.

514 [50] M. Panizza, G. Cerisola, Chem. Rev. 109 (2009) 6541-6569.

515 [51] A. Zapata, T. Velegraki, J.A. Sánchez-Pérez, D. Mantzavinos, M.I. Maldonado, S.
516   Malato, Appl. Catal. B: Environ. 88 (2009) 448-454.

517

Figure captions

519 **Fig. 1.** Front view of (a) the four filter-press type electrochemical cells of the pilot unit, and

520 (b) the CPC photoreactor. In (c), schematic diagram of the pilot unit equipped with one cell

521 (examined in this work), showing: (1) CPC photoreactor, (2) valve, (3) feed tank, (4) power

522 supply, (5) electrochemical reactor, (6) liquid flowmeter, (7) air compressor, (8) magnetic

523 pump.

524 **Fig. 2.** (a) Accumulated H_2O_2 concentration and current efficiency (% CE) at different pH

525 values and current densities (j). The values were obtained after 30 min of continuous

526 recirculation of a 50 mM Na_2SO_4 solution at a liquid flow rate of 4.4 L min^{-1} and air flow rate

527 of 5 L min^{-1}. (b) H_2O_2 production rate as function of electrolysis time, at constant pH = 3.0

528 and various j values. (c) H_2O_2 production rate as function of electrolysis time, at constant j =

529 100 mA cm^{-2} and varying pH.

530 **Fig. 3.** Comparison of the actual results obtained experimentally regarding (a) H_2O_2

531 production and (b) current efficiency (in %), with those predicted via central composite

532 design equations (12) and (13), respectively.

533 **Fig. 4.** (a) 3D surface plot and (b) contour plot for the H_2O_2 production as function of the

534 initial pH (A) and current density (B). Experimental data correspond to 30-min electrolyses

535 under continuous recirculation of a 50 mM Na_2SO_4 solution at liquid flow rate of 4.4 L min^{-1}

536 and air flow rate of 5 L min^{-1}.

537 **Fig. 5.** (a) 3D surface plot and (b) contour plot for current efficiency (in %), as in Fig. 4.

538 **Fig. 6.** (a) Effect of liquid flow rate on various process efficiency parameters, corresponding

539 to 30-min electrolyses; (b) accumulated H_2O_2 as a function of electrolysis time, at three

540 different liquid flow rates. Fixed parameters: 50 mM Na_2SO_4 at pH 3.0, $j = 74$ mA cm^{-2}, air

541 flow rate of 5 L min^{-1}.

542 **Fig. 7.** (a) Effect of air flow rate on various process efficiency parameters, corresponding to

543 30-min electrolyses; (b) accumulated H_2O_2 as function of electrolysis time, at different air

544 flow rates. Fixed parameters: 50 mM Na_2SO_4 at pH 3.0, $j = 74$ mA cm^{-2}, liquid flow rate of

545 4.4 L min^{-1}. The optimum trial corresponds to the same conditions but using a liquid flow rate

546 of 5.6 L min^{-1} and air flow rate of 10 L min^{-1}.

547 **Fig. 8.** (a) Effect of Na_2SO_4 molar concentration on various process efficiency parameters,

548 corresponding to 30-min electrolyses; (b) accumulated H_2O_2 as a function of electrolysis time,

549 at three different electrolyte concentrations. Fixed parameters: electrolyte solution at pH 3.0, j

550 $= 74$ mA cm^{-2}, liquid flow rate of 4.4 L min^{-1} and air flow rate of 5 L min^{-1}.

551 **Fig. 9.** Normalized concentration decays of pesticides (a) pyrimethanil (PYR) and (b)

552 methomyl (MET) versus electrolysis time during the (○,□) electro-oxidation (EO) and

553 (●,■) solar photoelectro-Fenton (SPEF) treatment of 75 L of mixtures of both pesticides (71

554 mg L^{-1} DOC) in deionized water with 50 mM Na_2SO_4 at pH 3.0 using the pilot plant at $j = 74$

555 mA cm^{-2}, liquid flow rate of 5.6 L min^{-1} and air flow rate of 10 L min^{-1}. SPEF treatment was

556 performed in the presence of 0.5 mM Fe^{2+} as catalyst.

557

558

559

560

561   **Fig. 1**
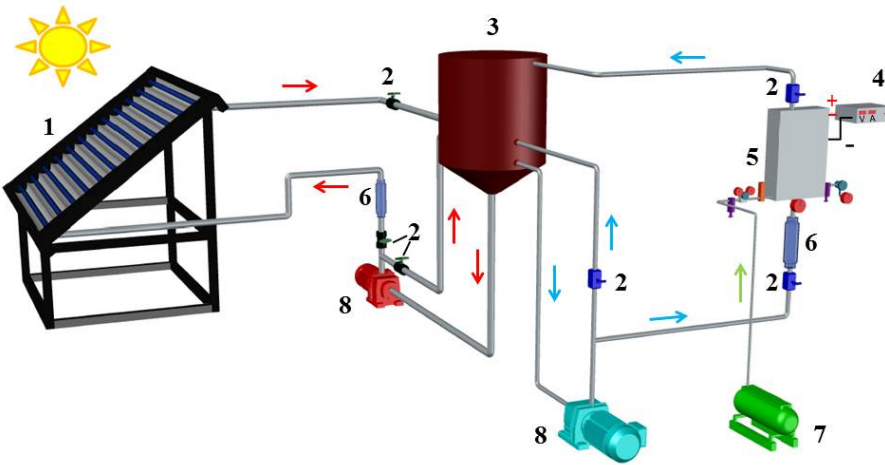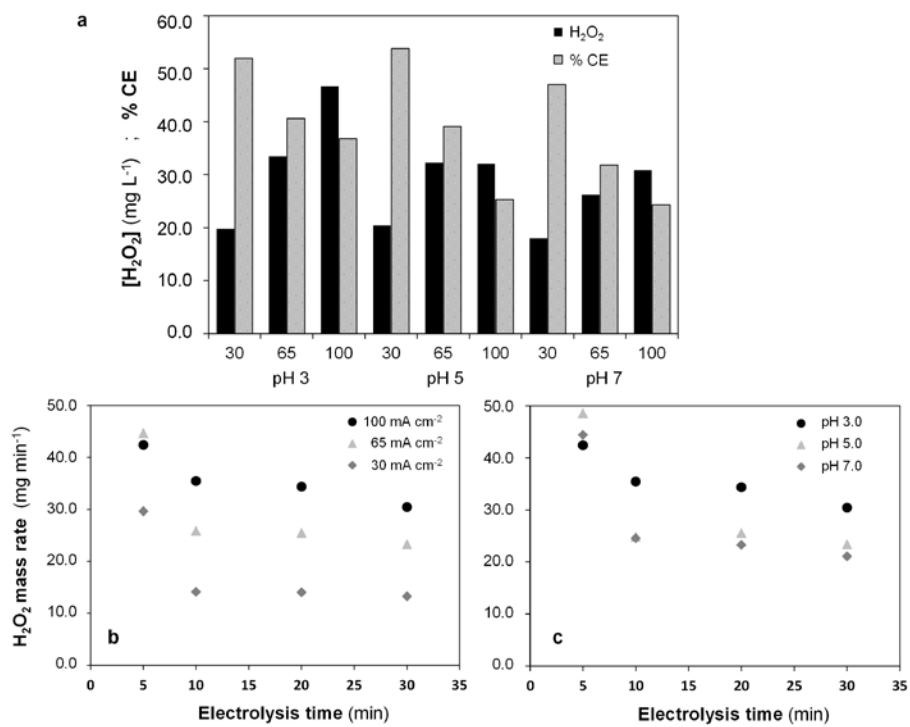
562

563
564
565
566
567
568   **Fig. 2**
569

-26-
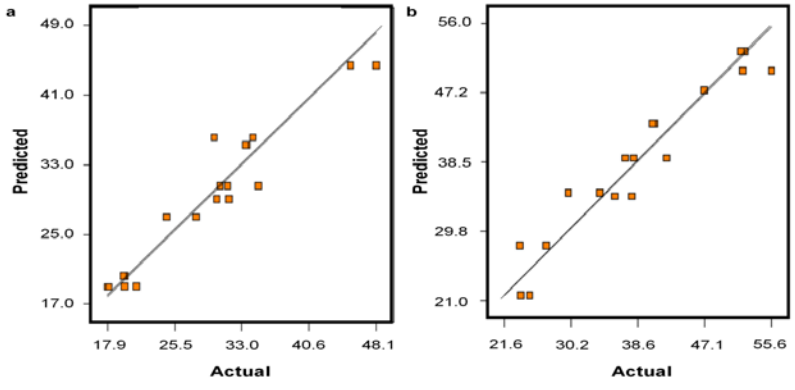
570

571

572

573

574

575   **Fig. 3**

576
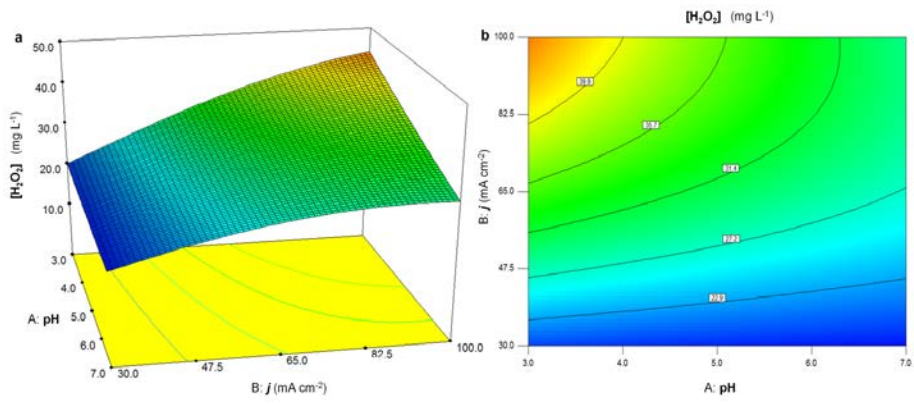
Fig. 4
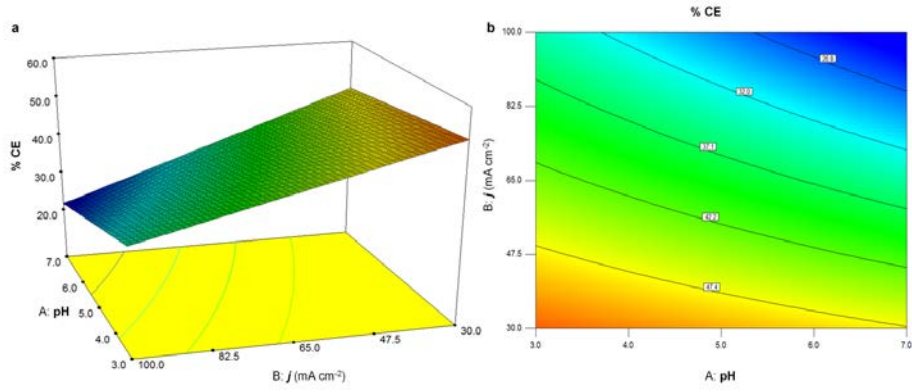
584

585

586

587

588

589   **Fig. 5**

590
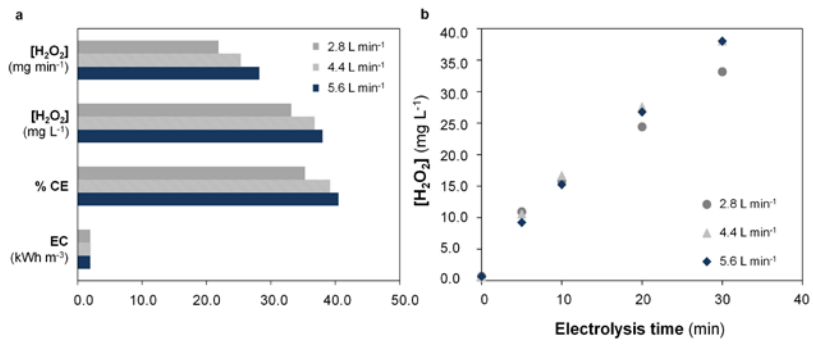
591

592

593

594

595

596

597   **Fig. 6**
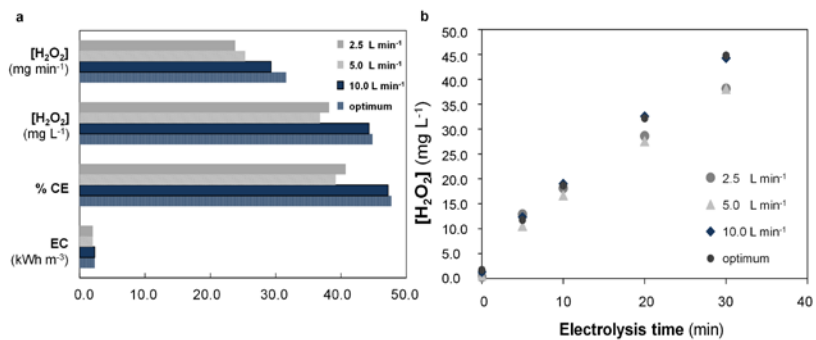
598

599

600

601

602

603   **Fig. 7**

604
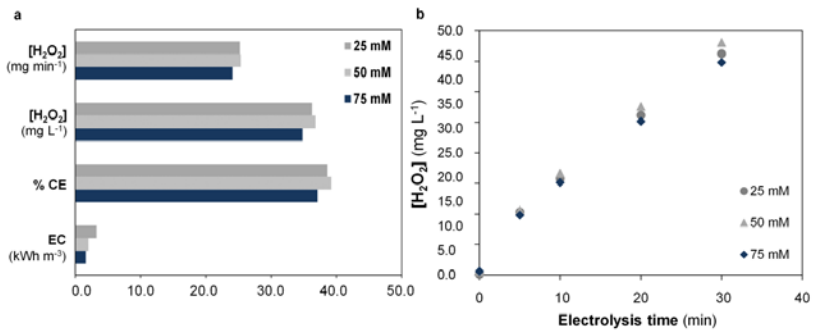
605

606

607

608

609

610   **Fig. 8**

611
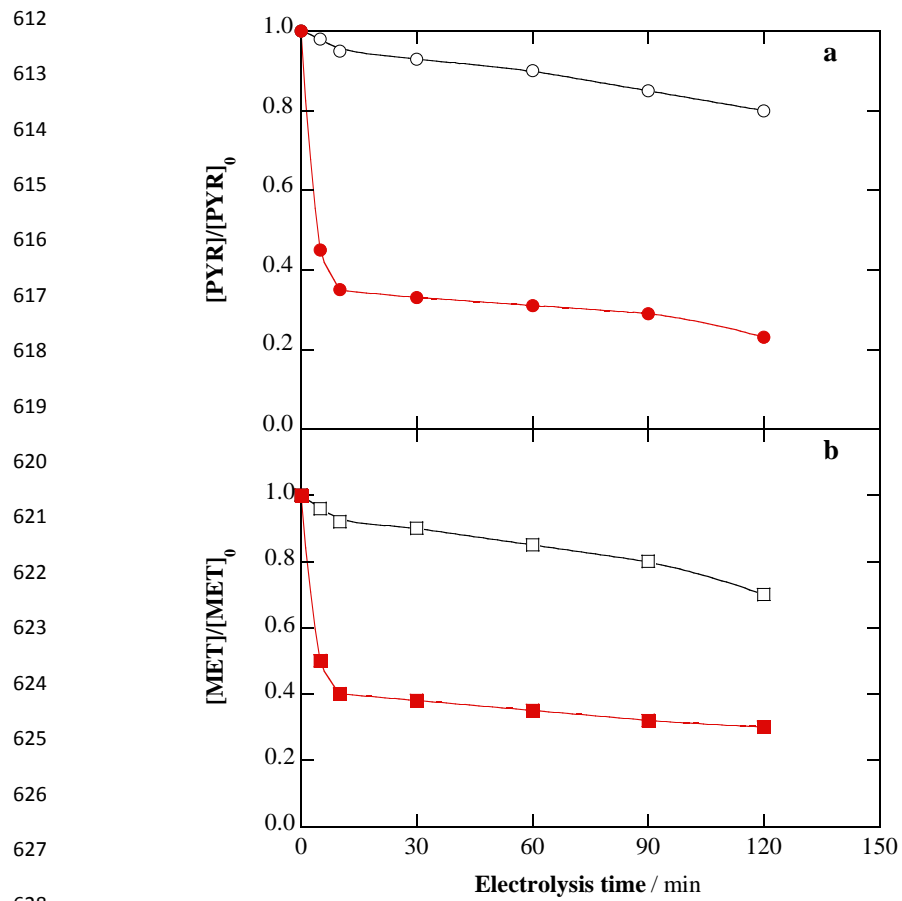
Fig. 9

634 **Table 1**

635 Experimental range and levels of independent variables

Variable	Factor	Units	Level and Range		
			Low (-1)	Central (0)	High (+1)
pH	A	-	3	5	7
j	B	mA cm^{-2}	30	65	100

636

637

638　**Table 2**

639　Design of experiments and results

Run	Independent variables		Responses (t = 5min)		Responses (t = 30min)	
	pH	j (mA cm^{-2})	[H_2O_2] (mg L^{-1})	% CE	[H_2O_2] (mg L^{-1})	% CE
1	3	100	15.11	71.40	48.12	37.90
2	7	30	4.97	78.30	18.06	47.05
3	5	65	10.41	75.70	34.85	42.30
4	7	100	8.88	42.00	31.55	24.90
5	3	30	5.93	93.40	19.67	51.70
6	3	100	13.41	63.40	45.25	35.70
7	5	65	9.23	67.20	31.42	38.10
8	5	100	9.71	45.90	34.25	27.00
9	3	65	8.93	65.00	33.59	40.70
10	7	100	8.45	40.00	30.16	23.80
11	5	100	8.36	39.60	29.90	23.60
12	5	30	6.23	98.20	21.15	55.60
13	5	65	8.67	63.10	30.55	37.00
14	5	30	5.49	86.60	19.80	52.00
15	3	30	5.75	90.70	19.85	52.20
16	7	65	7.71	56.10	27.85	33.80
17	3	65	9.67	70.30	33.38	40.50
18	7	65	6.58	47.90	24.54	29.80
19	7	30	4.84	76.30	17.89	47.00

640

641 **Table 3**

642 ANOVA results for response surface of the Quadratic and 2FI models

Source	Sum of squares	Degree of freedom	Mean square	F-value	p-value	
Quadratic model	1225.26	5	245.05	30.44	<0.0001	significant
A-pH	206.75	1	206.75	25.68	0.0002	
B-j	880.82	1	880.82	109.41	<0.0001	
AB	98.63	1	98.63	12.25	0.0039	
A^2	1.56	1	1.56	0.19	0.6673	
B^2	38.61	1	38.61	4.80	0.0474	
Residual	104.66	13	8.05			
Lack of fit	73.34	3	24.45	7.80	0.0056	not significant
Pure error	31.33	10	3.13			
2FI model	1723.02	3	574.34	60.89	<0.0001	significant
A-pH	228.38	1	228.38	24.21	0.0002	
B-j	1466.34	1	1466.34	155.45	<0.0001	
AB	28.31	1	28.31	3.00	0.1037	
Residual	141.49	15	9.43			
Lack of fit	102.41	5	20.48	5.24	0.0127	not significant
Pure error	39.08	10	3.91			

643

644

645 **Table 4**

646 Optimum operation conditions proposed by Design Expert 7.0.0 software to attain maximum

647 H_2O_2 concentration and current efficiency at 30 min of electrolysis.

Test number	pH	j (mA cm^{-2})	[H_2O_2] (mg L^{-1})	% CE	Desirability	
1	3.00	73.66	38.0961	41.0744	0.604	Selected
2	3.00	74.16	38.2467	40.9437	0.604	
3	3.00	72.82	37.8392	41.2949	0.604	
4	3.00	70.00	36.9532	42.0343	0.603	

648

649

650 **Table 5**

651 Models validation under optimum conditions, with experimental data obtained after 30 min of

652 electrolysis under continuous recirculation of 50 mM Na_2SO_4 solution at pH 3.0, 74 mA cm^{-2},

653 liquid flow rate of 3.3 L min^{-1} and air flow rate of 5 L min^{-1}. Two independent runs were

654 performed

	Run		Average actual	Predicted	Relative error
	a	b	values	values	(%)
H_2O_2 (mg L^{-1})	35.51	38.07	36.79	38.20	3.69
% CE	37.80	40.60	39.20	40.99	4.38

655